JOURNAL OF SOLID STATE CHEMISTRY 111, 26–32 (1994)

A Phosphoniobate with an Intersecting Tunnel Structure Related to Pyrochlore: $Rb_3Nb_5P_2O_{19}$

A. Leclaire, M. M. Borel, J. Chardon, and B. Raveau

Laboratoire CRISMAT, Associé au CNRS, ISMRA, Université de Caen, Boulevard du Maréchal Juin, 14050 Caen Cedex, France

Received August 2, 1993; accepted January 12, 1994

IN HONOR OF C. N. R. RAO ON HIS 60TH BIRTHDAY

A new phosphoniobate $Rb_3Nb_5P_2O_{19}$ with an intersecting tunnel structure has been synthesized. It crystallizes in the $R\bar{3}c$ space group with $a_H = 12.989(2)$ Å and $c_H = 53.912(6)$ Å. The host lattice, related to the pyrochlore framework, is built up from "Nb_6O_{27}" and "$Nb_3P_3O_{24}$" units which share their corners in the (001) planes, forming $|Nb_2PO_8|_\infty$ layers. These layers, connected through NbO_6 octahedra, delimit large cages along c which contain the rubidium ions. The cages are connected through hexagonal tunnels running along $(2\,1\,0)_H$. The relationships with pyrochlore and $Rb_{10}Nb_{29.2}O_{78}$ are studied.

INTRODUCTION

Recent studies of the niobium phosphates have shown the close relationships between these mixed frameworks and the pure octahedral host lattices. The niobium phosphate bronzes form a large family whose structures are characterized either by hexagonal tunnels or by pentagonal tunnels. This is the case for the monophosphate bronzes $ANb_3P_3O_{15}$ with A = K, Rb, Cs (1–3) that are closely related to the tetragonal tungsten bronze (4); for the phosphate niobium bronzes with hexagonal tunnels $(A_3Nb_6P_4O_{26})_n \cdot ANb_2PO_8$ with A = K, Na (5) that are closely related to the hexagonal tungsten bronzes (HTB) (6), and for the intergrowth tungsten bronzes (ITB) (7). This similarity to pure octahedral structures has also been observed very recently for a phosphoniobate $RbNb_2PO_8$ (8) whose structure corresponds to an ordered substitution of PO_4 tetrahedra for NbO_6 octahedra in the pure octahedral HTB framework. Curiously, no mixed framework derived from the pure octahedral pyrochlore host lattice has been obtained until now, in spite of the close relationships between HTB and pyrochlore structures. For this reason, we have more extensively investigated the Rb–Nb(V)–P–O system, especially in the region with higher Rb content. We report here the synthesis and structure of a new Nb(V) phosphate, $Rb_3Nb_5P_2O_{19}$, whose structure exhibits strong similarities with pyrochlore. The isotypic thallium phase was also synthesized.

SYNTHESIS AND CRYSTAL GROWTH

Single crystals of $A_3Nb_5P_2O_{19}$ (A = Rb, Tl) were extracted from mixtures of nominal composition ANb_2PO_8 (A = Rb, Tl). The latter were prepared from A_2CO_3, $H(NH_4)_2PO_4$, and Nb_2O_5 in appropriate proportions. The mixtures were mixed and heated to 873 K in a platinum crucible for 6 hr to decompose $H(NH_4)_2PO_4$ and A_2CO_3. The samples were heated in an evacuated silica ampoule at 1298 K for 24 hr; the ampoules were then cooled slowly (3.5 K hr^{-1}) to 1023 K. The samples were finally quenched to room temperature. From the resulting mixtures, some colorless hexagonal plates were extracted. Microprobe analysis of these crystals confirmed the composition $A_3Nb_5P_2O_{19}$, in agreement with the structure determination.

Single phase powder samples of $A_3Nb_5P_2O_{19}$ with A = Rb, Tl were prepared by solid state reaction in air from A_2CO_3, $H(NH_4)_2PO_4$, and Nb_2O_5, mixed in appropriate proportions. The mixtures were first heated in air in a platinum crucible to 653 K. After regrinding, the products were finally heated to 1273 K for 12 hr and quenched at room temperature.

Powder X-ray diffractograms registered with a PW 3710 Philips diffractometer were indexed in a hexagonal cell (Table 1) with parameters obtained from the single crystal study (Table 2).

STRUCTURE DETERMINATION

Two colorless hexagonal plates were selected for structure determination, with dimensions 0.116 × 0.090 × 0.026 mm and 0.064 × 0.038 × 0.019 mm for the rubidium and thallium phases, respectively. The cell parameters were determined and refined by diffractometric techniques at 294 K with a least-squares refinement based upon 25 reflections with $18° < \theta < 22°$ (Table 2).

The data were collected on a CAD 4 Enraf–Nonius diffractometer as reported in Table 3. Unfortunately, for $Tl_3Nb_5P_2O_{19}$, the small number of reflections with $I \geq 3$

0022-4596/94 $6.00

TABLE 1
Interreticular Distances for $Rb_3Nb_5P_2O_{19}$

h	k	l	d_{calc} (Å)	d_{obs} (Å)	I_0	h	k	l	d_{calc} (Å)	d_{obs} (Å)	I_0
1	0	4	8.636	8.631	27	1	1	21	2.387	2.388	3.
1	1	0	6.495	6.490	15.5	0	3	18	2.340	2.342	3.
1	1	3	6.108	6.103	8.5	2	3	11	2.283	2.285	3.
0	1	8	5.781	5.779	20.	0	2	22	2.246	2.246	5.
1	1	6	5.264	5.263	7.	0	0	24	2.246		
1	0	10	4.861	4.857	8.	5	0	2	2.242	2.241	1.
0	0	12	4.493	4.500	10.	3	3	6	2.105	2.105	3.
1	1	9	4.403	4.405	1.	1	2	23	2.053	2.050	5.
2	1	1	4.238	4.243	2.	2	4	7	2.049		
0	3	0	3.750	3.751	9.5	3	2	16	2.049		
0	1	14	3.643	3.645	39.5	3	1	20	2.040	2.040	13
0	3	6	3.460	3.461	31.	0	1	26	2.039		
2	2	0	3.247	3.250	17.5	4	2	8	2.027	2.028	16.5
2	2	3	3.196	3.200	79.5	1	4	15	2.027		
2	0	14	3.177	3.170	22.	1	5	2	2.015	2.014	8.
1	1	15	3.145	3.144	47.5	2	2	21	2.014		
1	3	1	3.115	3.114	100.	2	4	10	1.977	1.974	17.
2	2	6	3.054	3.052	15.	5	1	7	1.954	1.953	19
3	1	5	2.997	2.999	80.	4	2	11	1.950	1.949	24.
0	0	18	2.995			3	3	12	1.950		
2	1	13	2.969	2.976	31.5	1	3	22	1.927	1.927	4.5
0	2	16	2.890	2.884	21.6	0	3	24	1.927		
0	3	12	2.879	2.873	18.	3	2	19	1.909	1.909	3.
2	2	9	2.854	2.851	8.	1	4	18	1.899	1.900	3.
1	2	14	2.854			1	0	28	1.898		
3	1	8	2.831	2.829	8.	5	1	10	1.892	1.894	3.
4	0	4	2.753	2.749	12.5	2	4	13	1.892		
1	1	18	2.720	2.720	9.5	6	0	0	1.875	1.875	18.5
3	1	11	2.632	2.635	7.5	3	1	23	1.874		
2	2	12	2.632			0	5	16	1.871	1.870	10.
3	2	1	2.578	2.580	4.	2	3	20	1.864	1.864	4.5
2	3	2	2.569	2.570	4.5	1	2	26	1.864		

σ (I) (only 799) that could be collected did not allow the structure to be refined. The reflections of the rubidium phase were corrected for Lorentz, polarization, absorption (Gaussian method), and secondary extinction effects.

The structure was solved by the heavy atom method and refined by the full matrix least-squares method. The refinement of the atomic coordinates and their thermal anisotropic factors led to $R = 0.031$ and $R_W = 0.030$ and to the atomic parameters summarized in Table 4.

DESCRIPTION OF THE STRUCTURE AND DISCUSSION

The projection of the structure of $Rb_3Nb_5P_2O_{19}$ along [210] (Fig. 1a) shows that the host lattice $[Nb_5P_2O_{19}]_\infty$ consists of corner-sharing NbO_6 octahedra and PO_4 tetrahedra. In this framework, each PO_4 tetrahedron shares its four apices with four octahedra, whereas there exist four kinds of NbO_6 octahedra. The Nb(1)O_6 octahedra share their six apices with six NbO_6 octahedra, the Nb(2)O_6 octahedra are linked to three NbO_6 octahedra and three PO_4 tetrahedra, the Nb(3)O_6 octahedra share four apices with four NbO_6 octahedra and two PO_4 tetrahedra, and the Nb(4)O_6 octahedra are linked to five NbO_6 octahedra and one PO_4 tetrahedron.

TABLE 2
Crystallographic Parameters

Compound	a (Å)	b (Å)	c (Å)	γ(°)	V (Å^3)
$Rb_3Nb_5P_2O_{19}$	12.989(2)	12.989(2)	53.912(6)	120	7877(40)
$Tl_3Nb_5P_2O_{19}$	13.027(3)	13.027(3)	53.616(6)	120	7878(70)

The PO_4 tetrahedron has the classical geometry of monophosphate groups, as shown in Table 5. The "O_6" octahedra that ensure the coordination of Nb(V) are not strongly distorted. The mean Nb–O distance does not vary dramatically from one octahedron to the other (1.959 to 2.001 Å). On the other hand, a significant variation of this distance is observed by comparing one Nb–O–Nb bond with one Nb–O–P bond. For Nb(1), located on a $\bar{3}$ axis, one observes, of course, six identical Nb–O distances corresponding to Nb–O–Nb bonds. On the opposite, the other Nb–O–P bonds of Nb(2) are significantly larger (2.11 Å) than the three Nb–O–Nb bonds (1.888 Å)

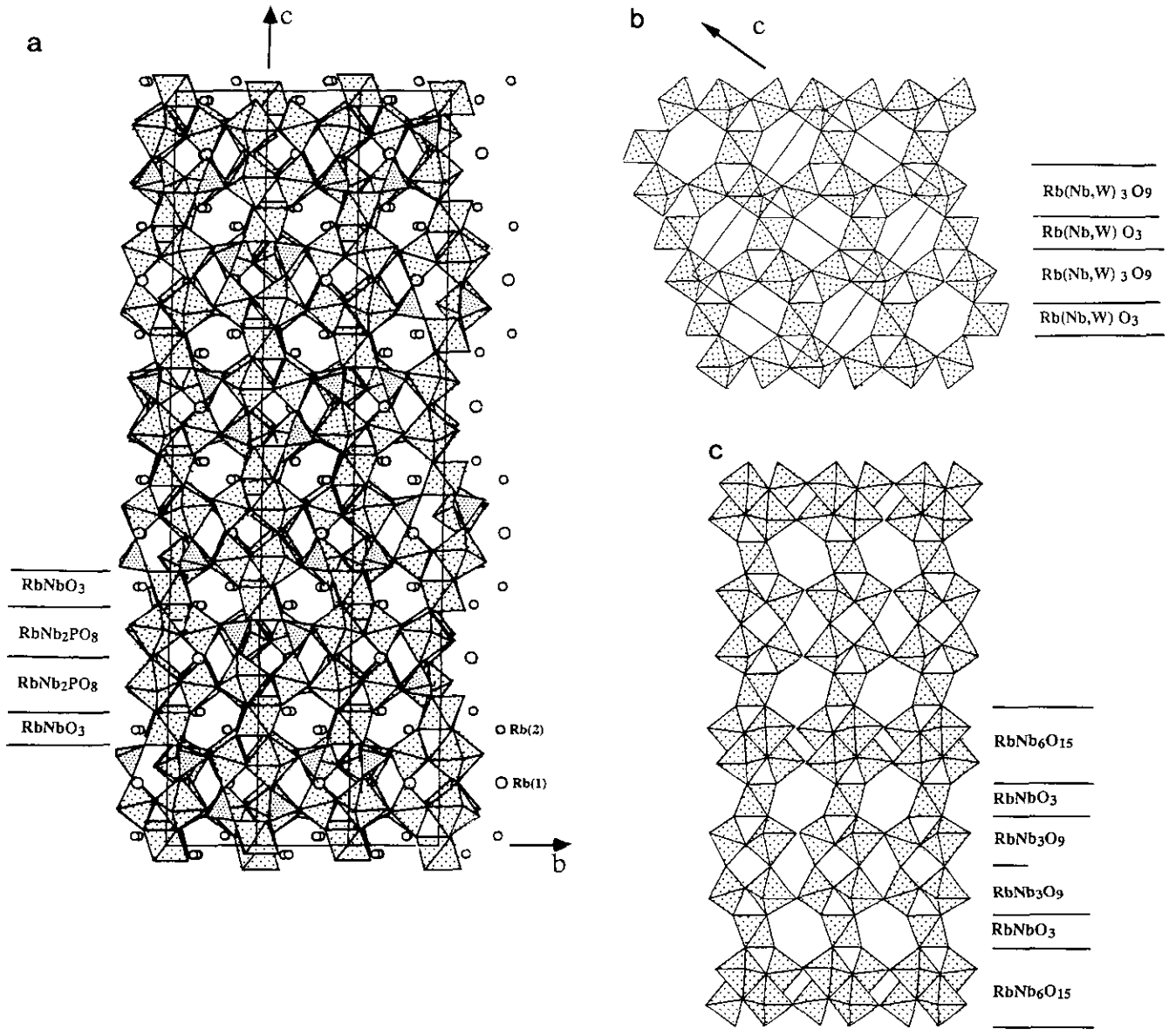

FIG. 1. The six-sided tunnels running along (a) $[210]_H$ in $Rb_3Nb_5P_2O_{19}$, (b) $[110]_H$ in pyrochlore, and (c) $[110]_H$ in $Rb_{10}Nb_{29.2}O_{78}$.

Similar behavior is observed for Nb(3) and Nb(4), which exhibit Nb–O–P bonds significantly larger than the Nb–O–Nb bonds (Table 5).

The $[Nb_5P_2O_{19}]_\infty$ framework can be described from two sorts of structural units: the octahedral blocks "Nb_6O_{27}" previously encountered in the intersecting tunnel structure $Rb_{10}Nb_{29.2}O_{78}$ (9) and the mixed octahedral–tetrahedral units "$Nb_3P_3O_{24}$" built up from three $Nb(3)O_6$ octahedra and three PO_4 tetrahedra. Along **c** these two kinds of units are linked through an $Nb(1)O_6$ or an $Nb(2)O_6$ octahedron whose ternary axis is parallel to **c**, forming columns (Fig. 2a) according to the sequence

$$[-Nb(1)-Nb_3P_3O_{24}-Nb(2)-Nb_6O_{27}-Nb(2)-Nb_3P_3O_{24}-Nb(1)-]_2.$$

In each column the successive Nb_6O_{27} (or $Nb_3P_3O_{24}$) blocks are related one to the other through the $\bar{3}$ axis that coincides with the axis of the column. Laterally, i.e., in the $(001)_H$ plane, three columns share the corners of their polyhedra, forming $[Nb_5P_2O_{23}]_\infty$ layers parallel to $(110)_H$ (Fig. 3) that exhibit two kinds of hexagonal windows, built up from four octahedra and two tetrahedra and from five octahedra and one tetrahedron, respectively. The stacking of the $[Nb_5P_2O_{23}]_\infty$ layers along $[110]_H$ leads to the tridimensional framework $[Nb_5P_2O_{19}]_\infty$; in this the hexagonal windows delimit tunnels running along $[210]_H$ (Fig. 1) and zig–zag tunnels parallel to **c** (Fig. 4).

In fact, this framework exhibits strong similarities with those of the pyrochlore $RbNbWO_6$ and of the niobate $Rb_{10}Nb_{29.2}O_{78}$ (9), as shown by the comparison of the

TABLE 3
Summary of Crystal Data, Intensity Measurements, and Structure Refinement Parameters for $Rb_3Nb_5P_2O_{19}$

1. Crystal data	
Space group	$R\bar{3}c$
Cell dimensions	a = 12.989 (2) Å
	b = 12.989 (2) Å γ = 120°
	c = 53.912 (6) Å
Volume	7877(3) Å^3
Z	18
$d_{calc.}$	4.12
$d_{exp.}$	4.07
2. Intensity measurements	
λ (Mo$K\alpha$)	0.71073 Å
Scan mode	$\omega - \frac{2}{3}\theta$
Scan width (°)	1 + 0.35 tan θ
Slit aperture (mm)	1.06 + tan θ
max θ (°)	38°
Standard reflections	3 (every 3000 sec)
Reflections with $I > 3\sigma$	2337
Measured reflections	10,064
μ (mm^{-1})	11.38
3. Structure solution and refinement	
Parameters refined	134
Agreement factors	R = 0.031, R_w = 0.030
Weighting scheme	$w = f(\sin\theta/\lambda)$
Δ/σ max	<0.004

$[210]_H$ projection (Fig. 1a) with those of these structure along $[110]_H$ (Figs. 1b,1c). The three structures are characterized by a similar disposition of the hexagonal tunnels running along $[210]_H$ in the phosphoniobate and along $[110]_H$ in the two other phases. The three structures contain identical $[RbNbO_3]_\infty$ layers involving the isolated Nb(1) and Nb(2) octahedra whose ternary axes are parallel to $\mathbf{c}_H$. They differ by the nature of the layers that are sandwiched between the $[RbNbO_3]_\infty$ layers. In the phosphoniobate one observes double $[RbNb_2PO_8]_\infty$ layers stacked with the $[RbNbO_3]_\infty$ layers according to the sequence $(RbNb_2PO_8)_2 \cdot RbNbO_3$ (Fig. 1a). In the pyrochlore, the double phosphoniobate layers are replaced by single HTB layers $[RbNb_3O_9]_\infty$ (Fig. 1b), so that the sequence $(RbNb_3O_9)$. $RbNbO_3$ is observed. In the niobate $Rb_{10}Nb_{29.2}O_{78}$ there exist two kinds of layers between the $RbNbO_3$ layers (Fig. 1c), double HTB $[RbNb_3O_9]_\infty$ layers and "sheared" HTB layers $[RbNb_6O_{15}]_\infty$, leading to the sequence $(RbNb_3O_9)_2 \cdot RbNbO_3 \cdot (RbNb_6O_{15}) \cdot RbNbO_3$. The similarity between the double HTB layers $[RbNb_3O_9]_2$ and the double phosphate layers $[RbNb_2PO_8]_2$ is also seen by considering the columns of polyhedra running along **c**

TABLE 4
Positional Parameters and Their Estimated Standard Deviations

Atom	x	y	z	B(Å^2)
Nb(1)	0.	0.	0.	0.83(2)
Nb(2)	0.	0.	0.15913(2)	0.54(1)
Nb(3)	0.16987(4)	0.14913(4)	0.05416(1)	0.530(8)
Nb(4)	0.01723(4)	0.16947(5)	0.21506(1)	0.784(9)
Rb(1)	0.6723(1)	0.	0.25	3.47(3)
Rb(2)	0.6529(1)	0.0031(1)	0.32112(2)	4.87(3)
P	0.2187(1)	0.2165(1)	0.11778(3)	0.46(2)
O(1)	0.1263(3)	0.1223(3)	0.02055(7)	0.79(8)
O(2)	0.1189(3)	0.1319(4)	0.13426(8)	1.00(8)
O(3)	0.0063(3)	0.1255(3)	0.17797(7)	0.73(7)
O(4)	0.1744(4)	0.2056(4)	0.40892(8)	1.35(9)
O(5)	0.1230(3)	−0.0095(3)	0.06028(8)	0.81(8)
O(6)	0.3314(3)	0.1957(3)	0.04485(8)	0.72(8)
O(7)	0.2189(4)	0.3299(4)	0.04840(9)	1.42(9)
O(8)	0.1325(3)	0.1256(3)	0.21878(8)	0.91(8)
O(9)	0.	0.1901(4)	0.25	0.9(1)
O(10)	−0.1041(3)	0.2272(3)	0.20524(8)	0.89(8)

Note. Anisotropically refined atoms are given in the isotropic equivalent displacement parameter, defined as $B = \frac{4}{3}[\beta_{11}a^2 + \beta_{22}b^2 + \beta_{33}c^2 + \beta_{12}ab\cos\gamma + \beta_{13}ac\cos\beta + \beta_{23}bc\cos\alpha]$.

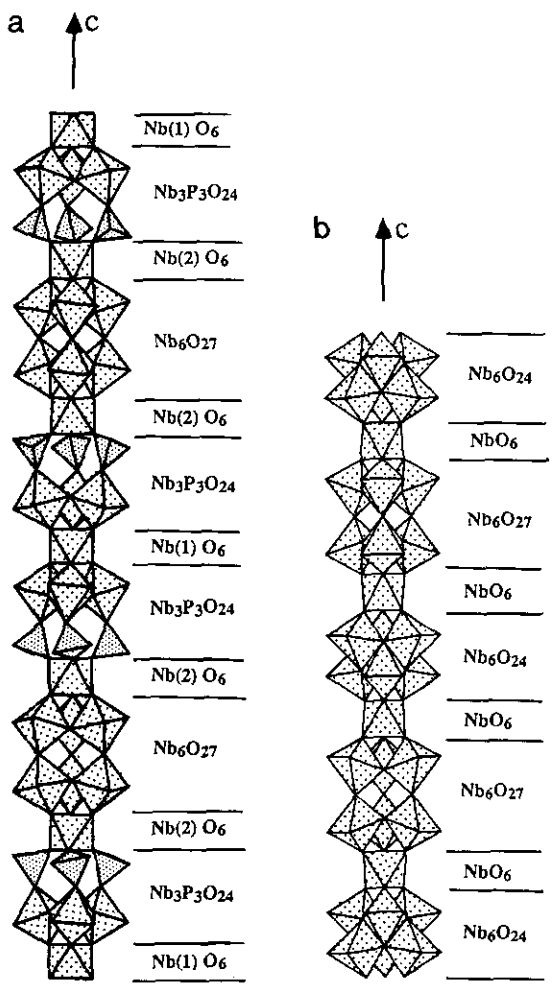

FIG. 2. (a) The $[Nb_5P_2O_{25}]_\infty$ column running along **c** in $Rb_3Nb_5P_2O_{19}$, built up from Nb_6O_{27} and $Nb_3P_3O_{24}$ blocks linked through NbO_6 octahedra; (b) the $[Nb_{14}O_{51}]_\infty$ column running along **c** in $Rb_{10}Nb_{29.2}O_{78}$, built up from Nb_6O_{27} and Nb_6O_{24} octahedral blocks linked through NbO_6 octahedra.

TABLE 5
Distances (Å) and Angles (°) in the Octahedra and Tetrahedra for $Rb_3Nb_5P_2O_{19}$

Nb(1)	O(1^{i})	O(1)	O(1^{ii})	O(1^{iii})	O(1^{iv})	O(1^{v})
O(1^{i})	1.959(1)	3.917(9)	2.742(9)	2.798(9)	2.742(9)	2.798(9)
O(1)	180.	1.959(1)	2.798(9)	2.742(9)	2.798(9)	2.742(9)
O(1^{ii})	91.2(2)	88.8(2)	1.959(1)	3.917(9)	2.798(9)	2.742(9)
O(1^{iii})	88.8(2)	91.2(2)	180.	1.959(1)	2.742(9)	2.798(9)
O(1^{iv})	91.2(2)	88.8(2)	91.2(2)	88.8(2)	1.959(1)	3.917(9)
O(1^{v})	88.8(2)	91.2(2)	88.8(2)	91.2(2)	180.	1.959(1)
Nb(2)	O(2)	O(2^{ii})	O(2^{iv})	O(3)	O(3^{ii})	O(3^{iv})
O(2)	2.115(5)	2.833(8)	2.833(8)	2.754(8)	3.990(8)	2.964(8)
O(2^{ii})	84.1(2)	2.115(5)	2.833(8)	2.964(8)	2.754(8)	3.990(8)
O(2^{iv})	84.1(2)	84.1(2)	2.115(5)	3.990(8)	2.964(8)	2.754(8)
O(3)	86.7(2)	95.4(2)	170.8(2)	1.888(5)	2.756(8)	2.756(8)
O(3^{ii})	170.8(2)	86.7(2)	95.4(2)	93.8(2)	1.888(5)	2.756(8)
O(^{iv})	95.4(2)	170.8(2)	86.7(2)	93.8(2)	93.8(2)	1.888(5)
Nb(3)	O(1)	O(4^{vi})	O(5)	O(5^{ii})	O(6)	O(7)
O(1)	1.879(5)	3.909(8)	2.729(8)	2.666(8)	2.681(8)	2.780(8)
O(4^{iv})	176.2(2)	2.035(5)	2.655(8)	2.855(8)	2.917(8)	3.009(8)
O(5)	93.7(2)	85.8(2)	1.863(5)	2.879(8)	2.812(8)	3.987(8)
O(5^{ii})	86.5(2)	89.8(2)	95.9(3)	2.011(5)	3.927(8)	2.722(8)
O(6)	89.3(2)	94.6(2)	95.5(2)	168.1(2)	1.937(5)	2.786(5)
O(7)	87.8(2)	92.7(2)	177.6(2)	82.2(2)	86.4(2)	2.125(5)
Nb(4)	O(3)	O(6^{vii})	O(8)	O(8^{ii})	O(9)	O(10)
O(3)	2.065(5)	2.992(9)	2.743(9)	2.740(9)	3.982(9)	2.802(9)
O(6^{ii})	96.8(2)	1.937(5)	2.718(9)	3.931(9)	2.772(9)	2.745(9)
O(8)	88.5(2)	91.4(2)	1.866(5)	2.907(9)	2.817(9)	3.972(9)
O(i^{ii})	84.6(2)	171.1(2)	97.5(3)	2.006(5)	2.697(9)	2.828(9)
O(9)	170.4(2)	91.6(2)	96.0(2)	86.4(2)	1.931(2)	2.922(9)
O(10)	84.0(2)	85.0(2)	171.2(2)	86.4(2)	92.1(2)	2.123(5)

P	O(2)	O(4^{vi})	O(7^{viii})	O(10^{ix})
O(2)	1.501(5)	2.524(6)	2.461(6)	2.461(6)
O(4^{vi})	113.4(3)	1.519(5)	2.487(6)	2.476(6)
O(7^{viii})	108.1(3)	108.1(3)	1.504(5)	2.538(6)
O(10^{ix})	107.9(3)	107.9(3)	110.8(3)	1.544(5)

Rb(1)–O(4^{x}) = 3.432(5)
–O(4^{xi}) = 3.432(5)
–O(5^{xii}) = 2.984(5)
–O(5^{xiii}) = 2.984(5)
–O(6^{xii}) = 3.263(5)
–O(6^{xiii}) = 3.263(5)
–O(7^{xiv}) = 3.490(5)
–O(7^{xv}) = 3.490(5)
–O(8^{xvi}) = 3.082(5)
–O(8^{xvii}) = 3.082(5)

Rb(2)–O(1^{xviii}) = 3.133(5)
–O(3^{xv}) = 2.959(5)
–O(6^{xii}) = 3.163(5)
–O(6^{xviii}) = 3.457(5)
–O(7^{xiv}) = 3.301(5)
–O(10) = 3.409(5)
–O(10^{xv}) = 3.122(5)

Symmetry code

i:	$-x$	$-y$	$-z$
ii:	$-y$	$x-y$	z
iii:	y	$-x+y$	$-z$
iv:	$-x+y$	$-x$	z
v:	$x-y$	x	$-z$
vi:	y	x	$\frac{1}{2}-z$
vii:	$\frac{1}{3}-y$	$\frac{2}{3}-x$	$\frac{1}{6}+z$
viii:	$\frac{1}{3}+x-y$	$\frac{2}{3}-y$	$\frac{1}{6}-z$
ix:	$\frac{2}{3}+x-y$	$\frac{1}{3}+x$	$\frac{1}{6}-z$
x:	$\frac{1}{3}+y$	$-\frac{1}{3}-x+y$	$\frac{2}{3}-z$
xi:	$\frac{2}{3}+x$	$\frac{1}{3}+x-y$	$-\frac{1}{6}+z$
xii:	$\frac{2}{3}+y$	$\frac{1}{3}-x+y$	$\frac{1}{3}-z$
xiii:	$\frac{1}{3}+x$	$-\frac{1}{3}+x-y$	$\frac{1}{6}+z$
xiv:	$\frac{2}{3}-x$	$\frac{1}{3}-y$	$\frac{1}{3}+z$
xv:	$\frac{1}{3}-x+y$	$-\frac{1}{3}+z$	$\frac{1}{6}+z$
xvi:	$1-y$	$x-y$	z
xvii:	$1-x$	$-x+y$	$\frac{1}{2}-z$
xviii:	$\frac{2}{3}-x+y$	$\frac{1}{3}-x$	$\frac{1}{3}+z$
xix:	$1-x+y$	y	$\frac{5}{2}+z$

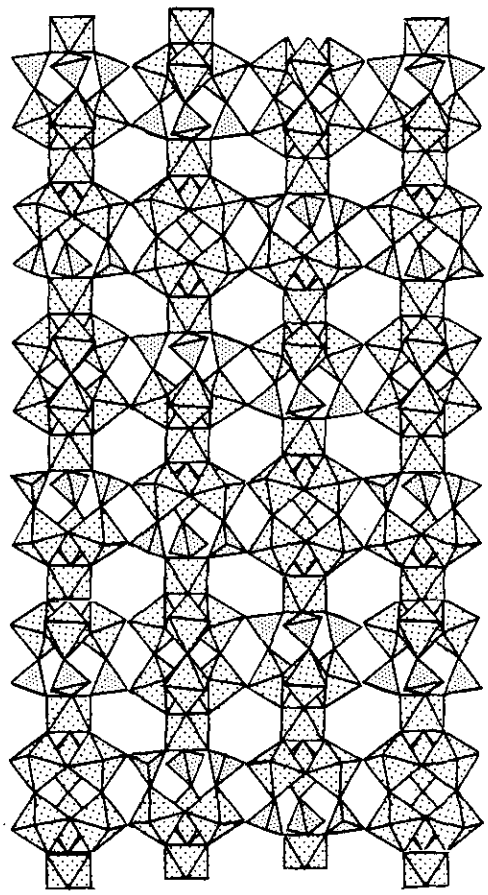

FIG. 3. The $[Nb_5P_2O_{23}]_\infty$ layers parallel to (110), showing two kinds of hexagonal windows.

(Fig. 2). The phosphoniobate layers exhibit two kinds of blocks, "Nb_6O_{27}" and "$Nb_3P_3O_{24}$" (Fig. 2a), whereas the double HTB layers of $Rb_{10}Nb_{29.2}O_{78}$ (Fig. 2b) can be described as built from "Nb_6O_{27}" units only.

The projections of one $[RbNb_2PO_8]_\infty$ layer along $\mathbf{c}_H$ (Fig. 5a), compared to those of the HTB $[RbNb_3O_8]_\infty$ layers observed in pyrochlore and in $Rb_{10}Nb_{29.2}O_{78}$ (Fig. 5b) and to the $[RbNb_6O_{15}]_\infty$ layers observed in the latter (Fig. 5c), show the great similarity of the three kinds of layers. It appears clearly that the $[RbNbO_8]_\infty$ layers exhibit HTB $[NbO_3]_\infty$ chains waving along $\mathbf{a}_H$ (Fig. 5a). However, their connection through PO_4 tetrahedra leads to seven-sided windows instead of the six-sided windows in pyrochlore or in $Rb_{10}Nb_{29.2}O_{78}$. The $[RbNb_2PO_8]_\infty$ layers of this new phase exhibit a different arrangement from that of the phosphoniobate $RbNb_2PO_8$ (8). One indeed observes from the projection of $RbNb_2PO_8$ structure along **b** (Fig. 5d) that this structure is also closely related to the HTBs, but it forms two kinds of windows: hexagonal windows limited by five NbO_6 octahedra and one PO_4 and heptagonal windows formed by four octahedra and three tetrahedra, whereas for $Rb_3Nb_5P_2O_{19}$ one observes one kind of heptagonal window involving five octahedra and two tetrahedra.

The double $[Nb_2PO_8]_\infty$ layers delimit two kinds of large cages where the rubidium ions are located (Fig. 4). These cages are connected through hexagonal tunnels running along $[210]_H$. The Rb(1) ions, surrounded by 10 oxygen atoms, are located at the centers of the hexagonal window in the double layers (Fig. 6). The Rb(2) ions, which exhibit a sevenfold coordination, are located at the level of Nb(1) and Nb(2) at the intersection of two [210] tunnels, at the boundary between the $[Nb_2PO_8]_\infty$ and $[NbO_3]_\infty$ layers.

CONCLUSION

A phosphoniobate closely related to the pure octahedral structures of pyrochlore and $Rb_{10}Nb_{29.2}O_{78}$ has been synthesized for the first time. The similarities between these oxides suggest that many other mixed frameworks derived from this structural type should be generated. The ion

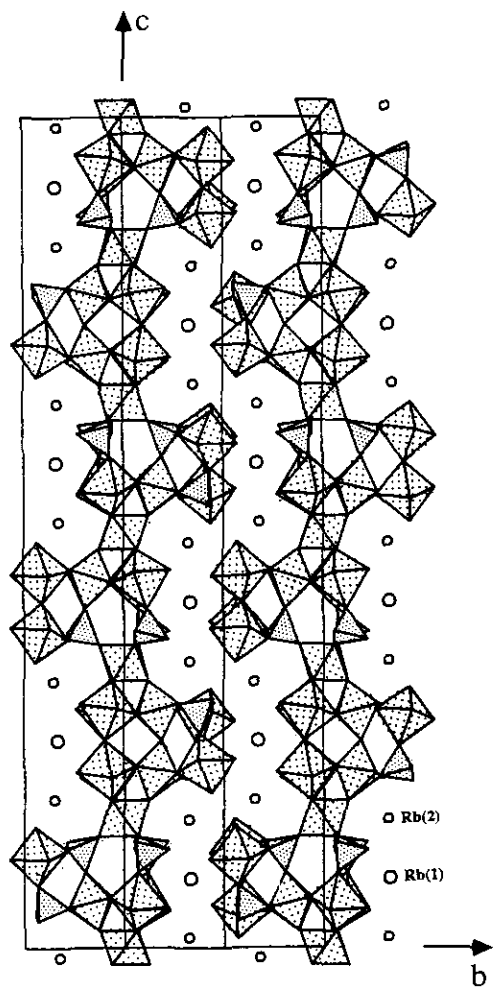

FIG. 4. The zig–zag tunnels running along **c** that contain the rubidium ions.

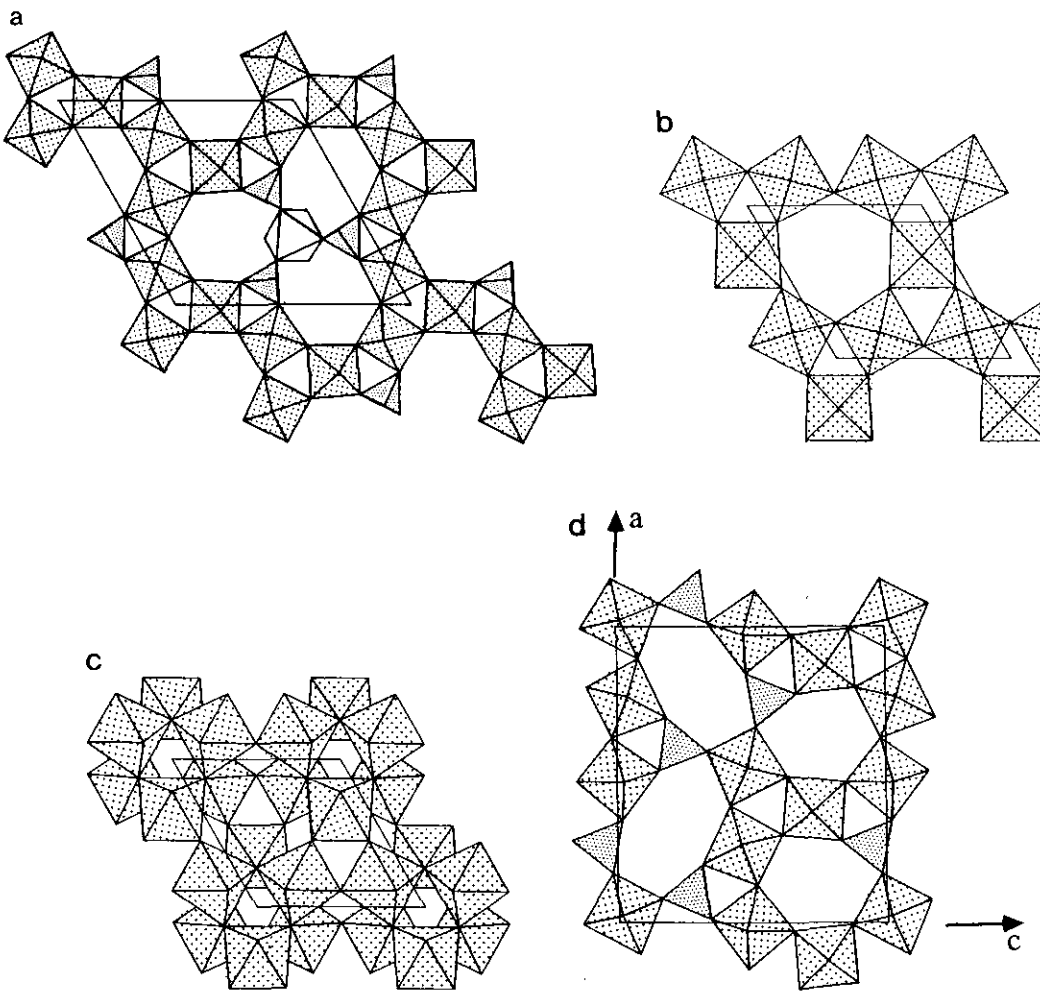

FIG. 5. (a) The $[RbNb_2PO_8]_\infty$ layer in $Rb_3Nb_5P_2O_{19}$ (the Rb atoms are omitted); (b) the HTB $[RbNb_3O_8]_\infty$ layeer in pyrochlore and in $Rb_{10}Nb_{29.2}O_{78}$; (c) the $[RbNb_6O_{15}]_\infty$ layer in $Rb_{10}Nb_{29.2}O_{78}$; (d) the $[RbNb_2PO_8]_\infty$ layer in $RbNb_2PO_8$.

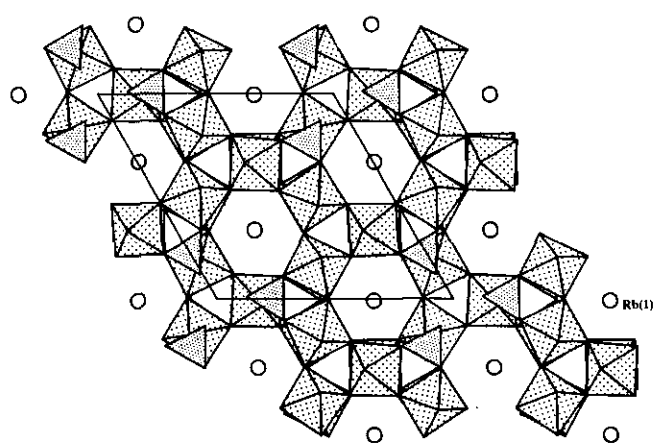

FIG. 6. The hexagonal windows containing Rb(1) in the $[RbNb_2PO_8]_\infty$ double layer.

exchange properties of this open structure will be investigated.

REFERENCES

1. A. Leclaire, M. M. Borel, A. Grandin, and B. Raveau, *J. Solid State Chem.* **80,** 12 (1989).
2. M. M. Borel, A. Benabbas, H. Rebbah, A. Grandin, A. Leclaire, and B. Raveau, *Eur. J. Solid State Inorg. Chem.* **27,** 525 (1990).
3. M. M. Borel, A. Grandin, G. Costentin, A. Leclaire, and B. Raveau, *Mater. Res. Bull.* **25,** 1155 (1990).
4. A. Magneli, *Arkiv. Kemi* **1,** 213 and 269 (1949).
5. B. Raveau, M. M. Borel, A. Leclaire, and A. Grandin, *Inter. J. Modern Phys.* **B7,** 4109 (1993).
6. A. Hussain and L. Kihlborg, *Acta Crystallogr. Sect. A* **32,** 551 (1976).
7. A. Benabbas, M. M. Borel, A. Grandin, A. Leclaire, and B. Raveau, *J. Solid State Chem.* **87,** 360 (1990).
8. A. Leclaire, M. M. Borel, A. Grandin, and B. Raveau, *J. Solid State Chem.*, in press.
9. C. Michel, A. Guyomarc'h, and B. Raveau, *J. Solid State Chem.* **25,** 251 (1978).